Cardiovascular Research (2011) **89**, 623–633
doi:10.1093/cvr/cvq351

Electrical remodelling precedes heart failure in an endothelin-1-induced model of cardiomyopathy

Erin E. Mueller[1], Abdul Momen[2], Stéphane Massé[2], Yu-Qing Zhou[3], Jie Liu[4], Peter H. Backx[4,5], R. Mark Henkelman[3,6], Kumaraswamy Nanthakumar[2,7], Duncan J. Stewart[1,7,8†‡], and Mansoor Husain[1,2,4,5,7*†]

[1]Department of Laboratory Medicine and Pathobiology, University of Toronto, Toronto, Ontario, Canada; [2]Toronto General Research Institute, Toronto, Ontario, Canada; [3]Mouse Imaging Centre, Hospital for Sick Children, Toronto, Ontario, Canada; [4]Heart and Stroke Richard Lewar Centre of Excellence in Cardiovascular Research, University of Toronto, Toronto, Ontario, Canada; [5]Department of Physiology, University of Toronto, Toronto, Ontario, Canada; [6]Department of Medical Biophysics, University of Toronto, Toronto, Ontario, Canada; [7]Department of Medicine, University of Toronto, Toronto, Ontario, Canada; and [8]Terrence Donnelly Heart Center, St Michael's Hospital, Toronto, Ontario, Canada

Received 24 February 2010; revised 29 October 2010; accepted 2 November 2010; online publish-ahead-of-print 9 November 2010

Time for primary review: 31 days

Aims Binary transgenic (BT) mice with doxycycline (DOX)-suppressible cardiac-specific overexpression of endothelin-1 (ET-1) exhibit progressive heart failure (HF), QRS prolongation, and death following DOX withdrawal. However, the molecular basis and reversibility of the electrophysiological abnormalities in this model were not known. Here, we assess the mechanisms underlying ET-1–mediated electrical remodelling, and its role in HF.

Methods and results BT vs. non-BT littermate controls were withdrawn from DOX and serially studied with ultrasound biomicroscopy, octapolar catheters, multielectrode epicardial mapping, histopathology, western blot, immunohistochemistry, and qRT–PCR. Abnormalities in ventricular activation and $-dV/dt$ were detected as early as 4 weeks after transgene activation, when the structure and function of the heart remained unaffected. By 8 weeks of ET-1 overexpression, biventricular systolic and diastolic dysfunction, myocardial fibrosis, and cardiomyocyte hypertrophy were observed. Intracardiac and epicardial electrograms revealed prolonged conduction and ventricular activation, reduced $-dV/dt$, and abnormal atrioventricular nodal function. Within 4 weeks of ET-1 induction, connexin 40 (Cx40) protein and Cx43 mRNA, protein, and phosphorylation levels were reduced by 36, 64, 93, and 69%, respectively; $Na_v1.5$ mRNA and protein levels were reduced by 30 and 50%, respectively, as was Na^+ channel conductance. Importantly, the associated electrophysiological abnormalities at this time point were reversible upon suppression of ET-1 overexpression and completely prevented the development of structural and functional remodelling.

Conclusion ET-1-mediated electrical remodelling correlates with reduced Cx40, Cx43, and $Na_v1.5$ expression and decreased Na^+ channel conductance and precedes HF. The sequence and reversibility of this phenotype suggest that a primary abnormality in electrical remodelling may contribute to the pathogenesis of HF.

Keywords Heart failure • Endothelin-1 • Cardiac electrophysiology • Connexins • Ion channels

1. Introduction

Endothelin-1 (ET-1), a 21 aa potent vasoconstrictive peptide, is implicated in the pathogenesis of several cardiovascular diseases such as heart failure (HF) and atherosclerosis.[1] ET-1 acts in an autocrine or paracrine fashion to participate in inflammation, fibrosis, cardiac hypertrophy, and electrical remodelling.[2] ET-1 has also been shown to play a role in disrupting gap-junctional intercellular communication[3–5] and to modulate ion channels.[6–10]

To investigate the role of ET-1 in the pathophysiology of cardiovascular disease, we developed a mouse model enabling temporal and spatial regulation of ET-1. We generated transgenic mice with conditional cardiac-specific overexpression of human ET-1 (hET-1) by crossing mice harbouring the tetracycline transactivator (tTA)

† The senior authors contributed equally to this work.

‡ Present address. Regenerative Medicine Program, Department of Medicine, Ottawa Hospital Research Institute, University of Ottawa, Ottawa, Ontario, Canada.

* Corresponding author: 101 College Street, TMDT East Tower, Rm 3-901, Toronto, ON, Canada M5G 1L7. Tel: +1 416 581 7488; fax: +1 416 581 7489, Email: mansoor.husain@utoronto.ca

Published on behalf of the European Society of Cardiology. All rights reserved. © The Author 2010. For permissions please email: journals.permissions@oup.com.

Downloaded from cardiovascres.oxfordjournals.org at University of Toronto Library on March 1, 2011

under control of the α-myosin heavy chain promoter, with a line harbouring a tTA-responsive, and thus doxycycline (DOX)-regulated (DOX-off), transgene for hET-1.[11] We have previously reported that this model is associated with an inflammatory cardiomyopathy characterized by increased cytokines, left ventricular (LV) dilatation, contractile dysfunction, progressive widening of QRS, HF, and death following DOX withdrawal.[11] What was not known is whether ET-1 was acting primarily as a cytokine-mediating inflammation and fibrosis or as a modulator of ion channel/electrical properties. We posited that this model provides a unique opportunity to assess the role of electrical remodelling in the initiation and progression of HF.

We now describe the temporal progression and precise nature of ET-1-induced electrical remodelling and determine that the subsequent development of a structural cardiomyopathy can be prevented by inhibiting further synthesis of ET-1 at a stage when only electrophysiological abnormalities are manifest.

2. Methods

2.1 Animals

Experiments conformed to protocols approved by the University Health Network Animal Use and Care Committee and to the Guide for Care and Use of Laboratory Animals (NIH Publication #85-23, revised 1996). Binary transgenic mice (BT: ET^+/tTA^+) and non-binary transgenic control littermates (NBT: ET^+/tTA^-; ET^-/tTA^+; ET^-/tTA^-) were administered DOX (200 mg/L) in drinking water from conception until weaning (3-week age). Experiments were conducted in mice withdrawn from DOX for 4 weeks (Group I), 8 weeks (Group II), or after 4 weeks of DOX removal with DOX re-administered for an additional 4 weeks (Group III, *Figure 1*). Following the acquisition of electrophysiological, haemodynamic, ultrasound biomicroscopy (UBM), or epicardial mapping data, mice were sacrificed by cervical dislocation. Hearts were either excised and snap frozen for RNA/protein extraction or perfusion-fixed for histopathology and immunohistochemistry.

2.2 Electrophysiology

Mice were anaesthetized with ip ketamine 100 mg/kg (MTC Pharmaceuticals, Cambridge, Ontario, Canada) and xylazine 10 mg/kg (Bayer Inc., Etobicoke, Ontario, Canada) and kept on a heating pad to maintain body temperature. Intracardiac electrograms were recorded with a 2 F octapolar electrode catheter (NuMED Inc., Hopkinton, NY, USA) to acquire atrial-His (AH) and His-ventricle (HV) intervals (*Figure 2A*). Atrioventricular Wenckebach (AV_{WENK}), 2:1 AV block cycle lengths ($AV_{2:1}$), and AV effective refractory periods (AV_{ERP}) were acquired during right atrial pacing.[12] Ventricular tachycardia (VT)/ventricular fibrillation (VF) induction was examined via right ventricular (RV) over-drive pacing and RV pacing with 12 basic stimuli followed by up to three extra decremental test steps as described.[12] Simultaneous surface electrocardiograms

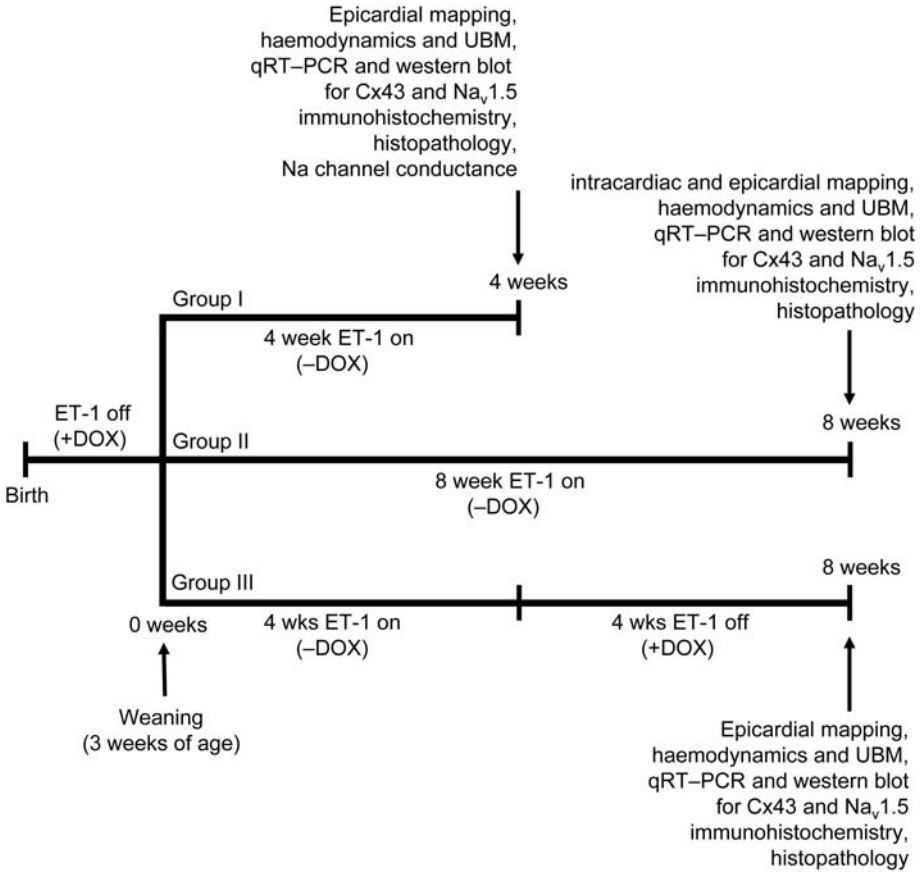

Figure 1 Schematic of experimental design. Mice were kept on DOX from conception until 3 weeks of age, then either withdrawn from DOX for 4 weeks (Group I), for 8 weeks (Group II), or withdrawn from DOX for 4 weeks followed by DOX re-administration for an additional 4 weeks (Group III). After the treatment periods, terminal experiments (intracardiac/epicardial mapping, ultrasound biomicroscopy, or LV invasive haemodynamics) were followed by histopathology, western blot, immunohistochemistry, and qRT–PCR on LV tissue samples.

Downloaded from cardiovascres.oxfordjournals.org at University of Toronto Library on March 1, 2011

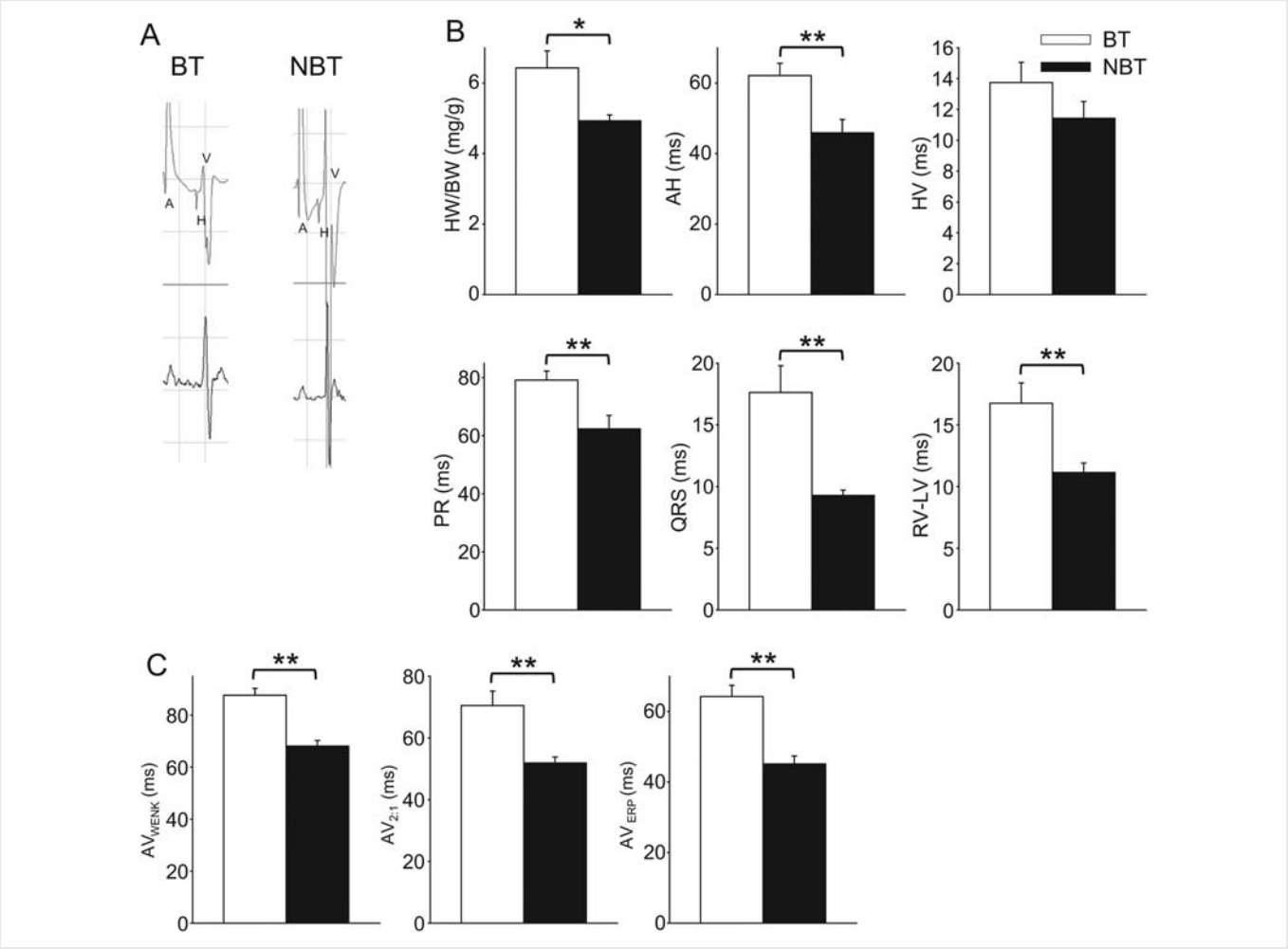

Figure 2 Electrophysiological evaluation reveals electrical defects in mice overexpressing ET-1 after 8–10 weeks of transgene induction. (*A*) Representative His bundle electrograms in BT vs. NBT mice. (*B*) Baseline conduction intervals, surface ECG parameters, HW/BW, and RV–LV conduction times in BT vs. NBT mice. (*C*) AV_{WENK}, $AV_{2:1}$, and AV_{ERP} in BT vs. NBT mice during RA pacing. *$P < 0.05$, **$P < 0.01$. BT, binary transgenic; NBT, non-binary transgenic; AH, atrial-His; HV, His-ventricle; AV_{WENK}, AV Wenckebach; $AV_{2:1}$, 2:1 AV block cycle lengths; AV_{ERP}, AV effective refractory periods.

(sECGs) were recorded to acquire PR, QRS, RR, and RV–LV intervals (from the onset of RV activation in intracardiac electrograms to the end of the QRS complex in the sECG). The heart weight to body weight ratio (HW/BW) was calculated as a measure of hypertrophy.

2.3 Haemodynamics

Pressure tracings were recorded in mice anaesthetized with isoflurane (1.5%) using a 1.4 F Millar catheter.[13] All data were analysed using an acquisition system (Sonometrics, London, Ontario, Canada).

2.4 Ultrasound biomicroscopy

A Vevo 770 (VisualSonics Inc., Toronto, Ontario, Canada) UBM with a transducer frequency of 30 MHz was used to acquire M-mode and Doppler recordings in mice anaesthetized with 1.5% isoflurane. Protocols to assess cardiac structures and function were as described.[14]

2.5 Epicardial mapping

Mice were anaesthetized with isoflurane (1.5%) and ventilated with air. Body temperature was maintained by a heating pad. Thoracotomy was performed to enable the application of a flexible 64 microelectrode array (4 × 16) with an interelectrode spacing of 800 μm on the epicardial surface (*Figure 3A*). The array was positioned around the heart in two orientations (*Figure 3B* and *C*). Unipolar electrograms were acquired with a custom-made software at 5k samples/s per channel, resulting in a time resolution of 0.2 ms, filtered with a high-pass and a low-pass filters of 0.5 and 1 kHz, and amplified with a gain of 500 using MEA1060 (Multi Channel Systems, Reutlingen, Germany). The sampling frequency was sufficient to determine the local activation time and generate accurate activation maps. A custom-made software was used to measure the atrial-to-ventricular activation time (*Figure 3B*), ventricular activation time, and ventricular activation with repolarization time (*Figure 3C*). Matlab (version 2007b) was used to calculate $-dV/dt$ and produce isochronal activation maps. The moment of local activity was determined as the time at which the electrogram signal increased significantly above background noise.

2.6 Quantitative real-time reverse-transcription–polymerase chain reaction

RNA from the LV was extracted using an ice-cold TRIzol reagent (Invitrogen, Burlington, Ontario, Canada), DNased, and reverse-transcribed with Superscript III (Invitrogen). cDNA was subjected to real-time PCR using

Downloaded from cardiovascres.oxfordjournals.org at University of Toronto Library on March 1, 2011

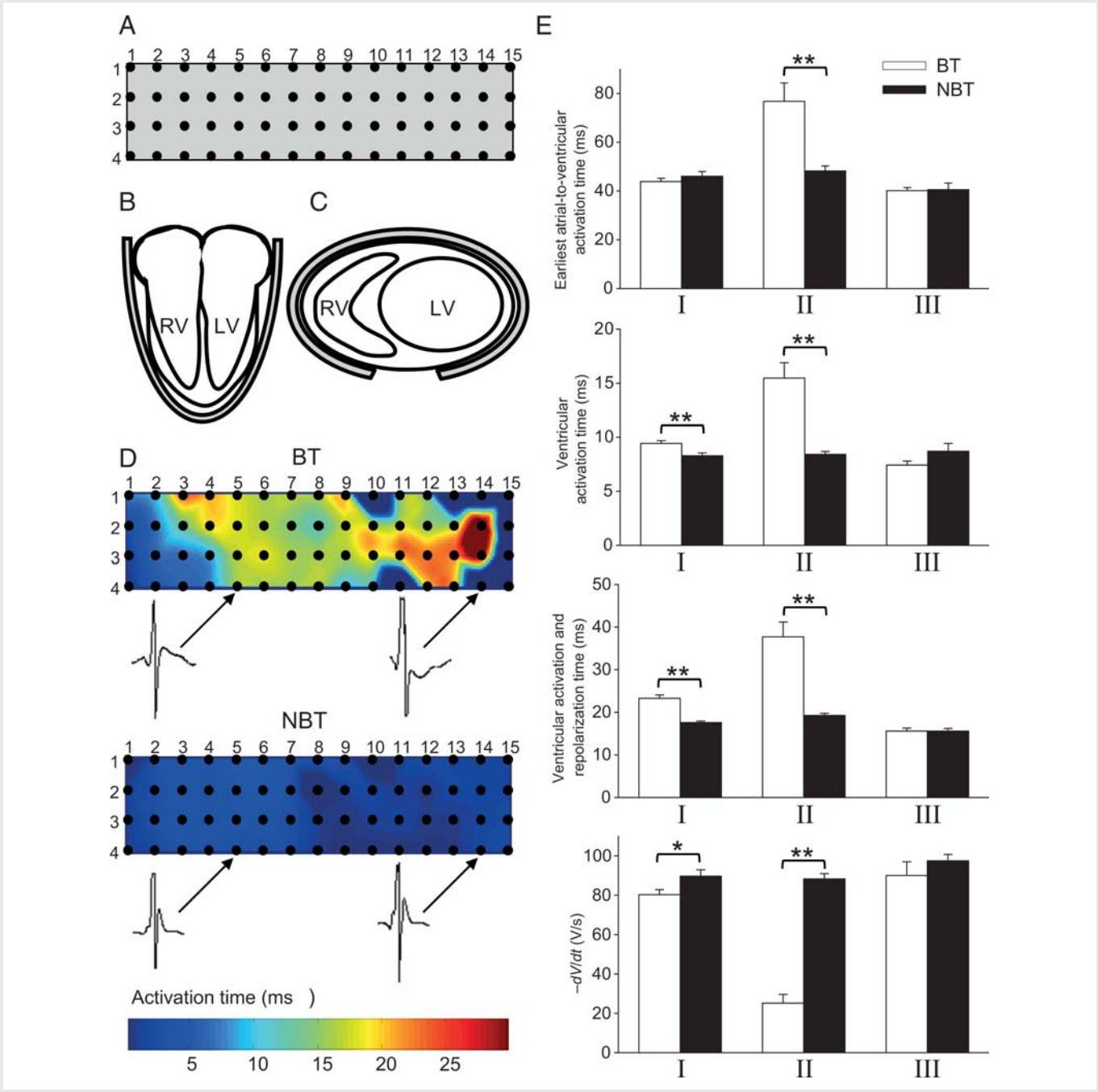

Figure 3 Temporal progression and prevention of electrical remodelling in mice overexpressing ET-1. Illustration of 4 × 16 microelectrode array (*A*), and placement of array while recording epicardial electrograms (*B* and *C*). (*D*) Ventricular isochronal activation maps in BT vs. NBT mice in Group II accompanied by representative epicardial electrograms from microelectrodes located at 4.5 and 4.14. (*E*) Earliest atrial-to-ventricular activation time, ventricular activation time, ventricular activation with repolarization time, and $-dV/dt$ measured in sinus rhythm in BT and NBT mice in Group I (BT: $n = 14$, NBT: $n = 24$), Group II (BT: $n = 21$ NBT: $n = 42$), and Group III (BT: NBT: $n = 7$). $^*P < 0.05$, $^{**}P < 0.01$.

the ABI Prism 7900 sequence detection system, version 2.3 (Applied Biosystems, Streetsville, Ontario, Canada), with SYBR green. Mouse-specific primers for GAPDH, IL−6, alpha-subunit of the cardiac Na^+ channel ($Na_v1.5$), connexin 40 (Cx40), Cx43, Cx45, alpaha1C-subunit of the L-type Ca^{2+} channel ($Ca_v1.2$), sarcoplasmic reticulum Ca^{2+} ATPase (SERCA2a), and primers for hET−1 were used[11,15–17] (see Supplementary material online, *Table S1*). Relative standard calibration curves were generated for each primer set with cDNA produced from one mouse heart. The mRNA level of each gene was normalized to that of GAPDH. All samples for each primer set were run together in duplicates.

2.7 Western blot

LV tissue was homogenized in ice-cold 1% SDS, 5 mM EDTA, 1 mM PMSF, 1× protease inhibitor cocktail, and 1× phosphatase inhibitor (Sigma-Aldrich, Oakville, Ontario, Canada). Twenty micrograms of protein extract were run on 4–12% SDS–PAGE, transferred to PVDF membrane, blocked in 5% non-fat dry milk in TBS-T (Tris base, NaCl, 0.1% Tween 20, pH 7.6) for 1 h, and incubated overnight at 4°C in TBS-T with 5% BSA containing primary rabbit Abs against Cx43 and phospho-Cx43 (p-Cx43) (Ser368; Cell Signaling, Danvers, MA, USA), Cx45 (Invitrogen),

Downloaded from cardiovascres.oxfordjournals.org at University of Toronto Library on March 1, 2011

Cx40 (Millipore, Billerica, MA, USA), $Na_v1.5$ (Sigma-Aldrich), and $Ca_v1.2$ (Alomone Laboratories, Jerusalem, Israel), or a primary mouse Ab against SERCA2a (Novus Biologicals, Littleton, CO, USA). Immunoreactivity was detected with chemiluminescence (Perkin Elmer, Woodbridge, Ontario, Canada), using a horseradish peroxidase-conjugated secondary goat anti−rabbit Ab (Pierce, Nepean, Ontario, Canada) in 5% non-fat dry milk in TBS-T for 30 min. Densitometry was performed using Quantity One (Bio-Rad, Hercules, CA, USA). GAPDH was used as a loading control to normalize protein samples. All samples from each group were run together.

2.8 Histopathology and immunohistochemistry

Details are provided in Supplementary material online. Sections were stained with Picrosirius Red. Fibrosis was quantified in three endocardial areas of the LV free wall from each section with ImageScope software (v9 algorithm, v10.2.2.2319, Aperio Technologies, Vista, CA, USA) to quantify the area of positively stained pixels. Cardiomyocyte cross-sectional area was measured at the level of the nucleus using Infinity Analyze (version 5.0.2, Lumenera Corporation, Ottawa, Ontario, Canada). Ten images from each Cx43- and p-Cx43-stained section were analysed with ImageScope to quantify the area of positively stained pixels.

2.9 Isolation of cardiomyocytes and patch-clamp recordings

These details are provided in Supplementary material online.

2.10 Statistical analysis

Data are presented as mean ± SE. Comparisons between BT vs. NBT in Groups I, II, or III were done by Student's *t*-tests using SPSS v12 (SPSS, Chicago, IL, USA).

3. Results

3.1 Electrical defects in mice with cardiac-specific ET-1 overexpression

All experimental groups studied and assays undertaken are summarized in *Figure 1*. To explore the electrophysiological basis for the QRS prolongation noted in our ET-1 overexpression model,[11] intracardiac mapping was performed in BT and NBT controls 8 weeks after withdrawal from DOX at weaning (*Figure 2A*). Confirming previous findings, PR, QRS, and HW/BW were increased in BT vs. NBT mice (*Figure 2B*). Invasive His bundle electrograms revealed that BT mice have slowed AH conduction, without affecting HV intervals (*Figure 2B*). Prolonged QRS in BT mice without significant changes in HV conduction was explained by prolonged RV−LV conduction time in BT vs. NBT littermates (*Figure 2B*). To investigate the basis of prolonged AH times in BT mice, we performed RA pacing and determined that AV_{WENK}, $AV_{2:1}$, and AV_{ERP} cycle lengths were prolonged in BT mice (*Figure 2C*). RV pacing protocols to provoke VT/VF failed to induce sustained ventricular arrhythmia in any Group II mice. These data suggest that the extensive AV nodal and interventricular conduction abnormalities are associated with chronic cardiac ET-1 overexpression.

3.2 Electrical remodelling is triggered as early as 4 weeks after ET-1 overexpression

Catheter size limitations in our system restrict intracardiac mapping to mice >20 g body weight. As such, this technique was not applicable in younger animals. Instead, a flexible multielectrode array was wrapped around the heart enabling epicardial mapping and characterization of the progression of specific electrophysiology parameters in ET-1 overexpressing mice as young as 4-week post-weaning (*Figure 3*). Earliest atrial-to-ventricular activation time (from the onset of right atrial activation to the onset of ventricular activation evaluated from one heart beat), ventricular activation time (from earliest-to-latest ventricular activation evaluated from one heart beat), ventricular activation and repolarization time (from earliest ventricular activation to latest ventricular repolarization acquired from one heart beat), and $-dV/dt$ (maximum negative rate of change of voltage in ventricular electrograms from one heart beat) were studied in sinus rhythm and during pacing. Significant ventricular conduction delays were observed as early as 4-week post-DOX withdrawal (Group I). Both ventricular activation time (9.4 ± 0.3 vs. 8.3 ± 0.3 ms, $P < 0.01$) and ventricular activation with repolarization time (23.3 ± 0.8 vs. 17.6 ± 0.3 ms, $P < 0.01$) were prolonged and $-dV/dt$ was reduced (80.3 ± 2.5 vs. 89.6 ± 3.2 V/s, $P < 0.05$) in BT vs. NBT mice in sinus rhythm (*Figure 3E*) and after pacing for 160 ms (data not shown).

Consistent with data obtained from intracardiac catheters, BT mice 8 weeks after DOX withdrawal (Group II) manifest more substantive abnormalities. Earliest atrial-to-ventricular activation time (76.8 ± 7.6 vs. 48.2 ± 2.0 ms, $P < 0.01$), ventricular activation time (15.5 ± 1.4 vs. 8.4 ± 0.3 ms, $P < 0.01$), as well as ventricular activation and repolarization time (37.7 ± 3.5 vs. 19.3 ± 0.5 ms, $P < 0.01$) were all prolonged, and $-dV/dt$ (25.2 ± 4.4 vs. 88.2 ± 2.7 V/s, $P < 0.01$) was reduced, in BT vs. NBT mice in sinus rhythm (*Figure 3D* and *E*) and after pacing for 160 ms (data not shown). Together, these results suggested that ET-1 mediates a progressive decline in ventricular conduction.

3.3 HF develops by 8 weeks of ET-1 overexpression

UBM and LV haemodynamics were used to study heart function in mice 4- to 8-week post-DOX withdrawal. Systolic blood pressure (SBP), LVSP, $+dP/dt$, and $-dP/dt$ were assessed by Millar catheters (*Table 1*), whereas peak velocity of blood flow in the main pulmonary artery and aorta, peak RV and LV *E*/*A* ratios, and FS% were evaluated by UBM (*Table 2*). No obvious structural/functional differences were observed in BT mice after 4 weeks of ET-1 overexpression (Group I). In contrast, and consistent with 'clinical' evidence of HF, BT mice exhibited severe structural and functional abnormalities by 8 weeks of transgene induction (Group II, *Tables 1* and *2*). LV systolic dysfunction was exemplified by reduced SBP (78.7 ± 1.5 vs. 96.1 ± 2.4 mmHg, $P < 0.01$), peak velocity of aortic flow (655 ± 91 vs. 943 ± 34 mm/s, $P < 0.01$), FS% (14.4 ± 2.4 vs. 27.0 ± 1.7, $P < 0.01$), and $+dP/dt$ (1214 ± 222 vs. 2728 ± 137 mmHg/s, $P < 0.01$) (*Tables 1* and *2*). LV diastolic dysfunction was manifest as reduced $-dP/dt$ (1578 ± 246 vs. 3198 ± 24 mmHg/s, $P < 0.01$) and elevated peak LV *E*/*A* ratio (10.8 ± 2.2 vs. 1.5 ± 0.1, $P < 0.01$) (*Tables 1* and *2*). Significant RV systolic (reduced flow in the main pulmonary artery; 404 ± 38 vs. 686 ± 68 mm/s, $P < 0.01$) and diastolic dysfunction (elevated peak RV *E*/*A* ratio; 6.5 ± 1.0 vs. 0.6 ± 0.0, $P < 0.01$) was also observed (*Table 2*). The development of HF also correlated with increased interleukin−6 mRNA expression, reduced Cx45 mRNA expression with no appreciable difference at the protein level, and reduced SERCA2a mRNA and protein expression (*Figure 4A*, *B*, *E*, *F*, and *M*). Consistent with these results, histopathology of heart sections from mice 4- and 8-week post-ET-1

Downloaded from cardiovascres.oxfordjournals.org at University of Toronto Library on March 1, 2011

Table 1 Progression and prevention of cardiac structural and functional abnormalities as evaluated by invasive haemodynamics

Parameter	Group I		Group II		Group III	
	BT ($n = 5$)	NBT ($n = 10$)	BT ($n = 6$)	NBT ($n = 4$)	BT ($n = 3$)	NBT ($n = 4$)
HW/BW (mg/g)	4.78 ± 0.19	4.91 ± 0.10	8.24 ± 0.66*	5.83 ± 0.23	7.47 ± 0.95	6.50 ± 0.33
SBP (mmHg)	99.6 ± 4.7	91.9 ± 2.1	78.7 ± 1.5**	96.9 ± 3.3	99.7 ± 2.5	107.0 ± 4.7
LVSP (mmHg)	108.6 ± 8.5	94.9 ± 3.2	66.5 ± 7.1*	94.2 ± 2.0	110.6 ± 1.3	110.7 ± 5.2
+d*P*/d*t* (mmHg/s)	2255 ± 170	2572 ± 146	1214 ± 222**	2778 ± 180	2452 ± 128	2548 ± 96
−d*P*/d*t* (mmHg/s)	2703 ± 207	2872 ± 145	1578 ± 246**	3198 ± 42	3422 ± 298	3585 ± 183

HW/BW, heart weight to body weight ratio; SBP, arterial systolic blood pressure; LVSP, LV systolic blood pressure; ± d*P*/d*t*, peak positive and negative first derivatives of the LV pressure.
*$P < 0.05$.
**$P < 0.01$.

Table 2 Progression and prevention of cardiac dysfunction as evaluated by ultrasound biomicroscopy

Parameter	Group I		Group II		Group III	
	BT ($n = 6$)	NBT ($n = 6$)	BT ($n = 6$)	NBT ($n = 6$)	BT ($n = 4$)	NBT ($n = 4$)
MPA PV (mm/s)	702 ± 14	735 ± 41	404 ± 38**	686 ± 68	815 ± 45	742 ± 36
Ao PV (mm/s)	945 ± 39	790 ± 70	655 ± 91**	944 ± 35	980 ± 28	1057 ± 82
RV *E/A*	0.60 ± 0.03	0.67 ± 0.12	6.54 ± 0.97*	0.59 ± 0.02	0.68 ± 0.05	0.68 ± 0.01
LV *E/A*	1.68 ± 0.09	1.59 ± 0.15	10.77 ± 2.17**	1.55 ± 0.08	2.02 ± 0.23	1.60 ± 0.13
FS%	28.2 ± 0.7	29.4 ± 1.4	14.4 ± 2.4**	27.0 ± 1.7	26.3 ± 1.1	24.8 ± 2.1

MPA, main pulmonary artery; PV, peak velocity; Ao, aorta; RV, right ventricle; *E/A*, ratio of peak early to atrial diastolic inflow velocities; FS, fractional shortening.
*$P < 0.05$.
**$P < 0.01$.

overexpression showed that fibrosis (6.4 ± 0.5 vs. 1.1 ± 0.1%, $P < 0.01$) (*Figure 5*) and hypertrophy (3793 ± 74 vs. 3540 ± 69 μm^2, $P < 0.01$; BT: $n = 223$ vs. NBT: $n = 244$ cells) were present only after 8 weeks of ET-1 overexpression.

3.4 ET-1-mediated electrical remodelling correlates with reduced Cx43, p-Cx43, Cx40, $Na_v1.5$, and Na^+ channel conductance

To define the molecular basis for ET-1-induced electrical remodelling, we examined the mRNA/protein expression levels of genes involved in action potential generation and propagation through the myocardium (*Figure 4*). Western blot analysis revealed that total Cx43 protein, p-Cx43 to total Cx43 protein ratio, and Cx40 protein were reduced by 93, 69, and 36%, respectively, in BT vs. NBT mice as early as 4-week post-ET-1 overexpression (Group I, *Figure 4H*, *L*, and *N*). qRT–PCR showed that high levels of hET-1 (transgene) mRNA expression also correlated with significantly reduced mRNA levels of $Ca_v1.2$ (72%), Cx40 (63%), Cx43 (64%), and $Na_v1.5$ (30%) by 4 weeks of transgene induction (Group I, *Figure 4C*, *G*, *I*, and *K*). At 8 weeks of ET-1 overexpression, $Ca_v1.2$, Cx40, Cx43, Cx45, and $Na_v1.5$ mRNA expression were reduced by 72, 69, 88, 61, and 64%, respectively (Group II, *Figure 4C*, *E*, *G*, *I*, and *K*), with the p-Cx43 to total Cx43 protein ratio, $Ca_v1.2$, Cx40, and $Na_v1.5$ protein levels being 54, 69, 54, and 71% lower in BT vs. NBT mice (Group II, *Figure 4D*, *H*, *J*, and *N*).

Immunohistochemistry was performed to explore the nature of disordered Cx43 expression. In agreement with western blot data, Cx43 and p-Cx43 stainings were greatly reduced in BT mice after only 4 weeks of ET-1 overexpression when compared with NBT controls (Cx43: 3.7 ± 0.3 vs. 9.9 ± 1.1%, $P < 0.01$; p-Cx43: 2.2 ± 0.3 vs. 7.8 ± 0.6%, $P < 0.01$) and further reduced after 8 weeks of ET-1 overexpression (Cx43: 0.2 ± 0.0 vs. 7.9 ± 0.2%, $P < 0.01$; p-Cx43: 0.2 ± 0.0 vs. 6.3 ± 0.3%, $P < 0.01$) (*Figure 6*). Furthermore, improper localization (i.e. lateralization) of Cx43 and p-Cx43 was observed in BT mice at the earliest stage (4 weeks, Group I), which became most severe with more prolonged ET-1 overexpression (8 weeks, Group II) (*Figure 6A* and *B*). Confirming the ability of ET-1 to directly reduce Cx43 levels in our model, exogenous ET-1 (10 nM) reduced Cx43 expression in neonatal mouse ventricular myocytes *in vitro* (see Supplementary material online, *Figure S1*).

To determine the functional consequence of reduced $Na_v1.5$ expression, Na current was recorded in LV myocytes isolated from mice 4 weeks post-DOX withdrawal (Group I). Na^+ channel conductance was reduced (0.17 ± 0.01 vs. 0.21 ± 0.01 s, $P < 0.05$) with no difference in cell capacitance (133.94 ± 8.50 vs. 126.50 ± 7.37 pF, P = NS) in BT ($n = 18$) vs. NBT ($n = 24$) (see Supplementary material online, *Figure S2*).

Downloaded from cardiovascres.oxfordjournals.org at University of Toronto Library on March 1, 2011

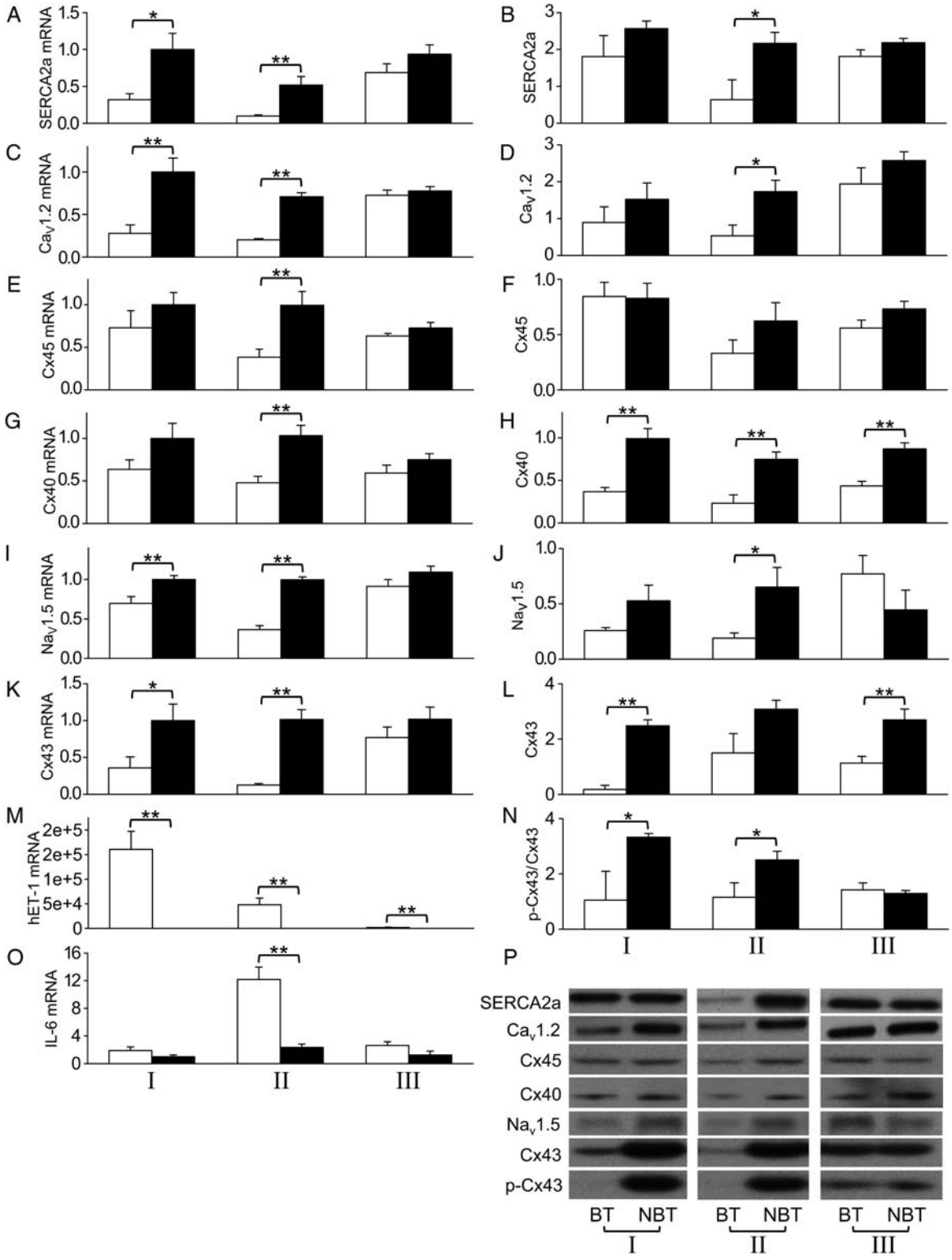

Figure 4 Reduced LV Cx43, Cx40, and $Na_v1.5$ expression in mice as early as 4 weeks after ET-1 induction. mRNA and protein expression of SERCA2a (*A* and *B*), $Ca_v1.2$ (*C* and *D*), Cx45 (*E* and *F*), Cx40 (*G* and *H*), $Na_v1.5$ (*I* and *J*), and Cx43 (*K* and *L*); as well as hET-1 mRNA (*M*), p-Cx43/total Cx43 protein (*N*), IL-6 mRNA (*O*), and representative western blots of LV of BT and NBT mice within Groups I–III (*P*). $n = 6–8$ for qRT–PCR, and $n = 3–6$ for western blot, for each genotype per group. $^*P < 0.05$, $^{**}P < 0.01$. SERCA2a, sarcoplasmic reticulum Ca^{2+}–ATPase; $Ca_v1.2$, α1C–subunit of the L-type Ca^{2+} channel; Cx, connexin; $Na_v1.5$, α-subunit of the cardiac Na^+ channel; hET-1, human–ET-1; IL-6, interleukin-6.

Downloaded from cardiovascres.oxfordjournals.org at University of Toronto Library on March 1, 2011

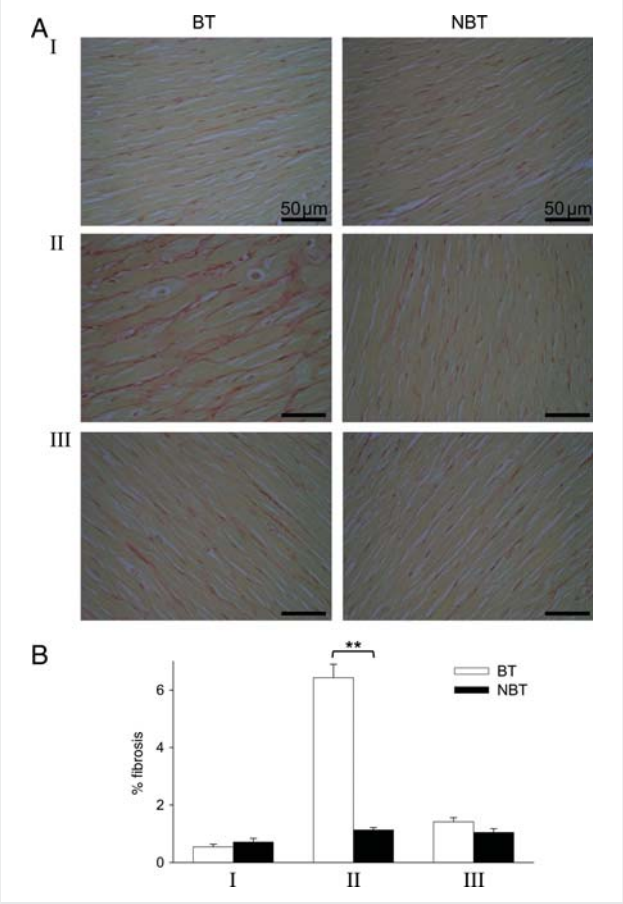

Figure 5 Myocardial fibrosis appears after 8 weeks of ET-1 overexpression. Representative Picrosirius Red-stained heart sections (*A*) and % fibrosis (*B*) from BT and NBT mice in Groups I–III ($n = 4–5$ per genotype per group). $^{**}P < 0.01$.

3.5 Inhibiting ET-1 expression at the onset of electrical remodelling prevents progression to HF

To determine whether inhibiting synthesis of ET-1 at the onset of ET-1-induced electrical remodelling will be effective in preventing the lethal phenotype, DOX was re-introduced 4 weeks after transgene induction and maintained for 4 weeks. At the end of this period, epicardial mapping, UBM, haemodynamics, histopathology, western blot, immunohistochemistry, and qRT–PCR were used to evaluate the effects of therapy. Re-introducing DOX at the onset of electrical remodelling completely prevented the development of the electrical, structural, and functional decline seen with age-matched BT mice maintained off DOX (*Figures 3* and *4*; *Tables 1* and *2*). Importantly, the reduced expression levels of Cx43 and $Na_v1.5$ that correlated with the onset of electrical remodelling at 4 weeks of ET-1 overexpression were nearly all normalized with re-administration of DOX (*Figures 4* and *6*). These data suggest that in this unique model, electrical remodelling precedes overt manifestations of HF and that the latter may be prevented by the reversal of the former.

4. Discussion

Cardiac electrical remodelling has traditionally been considered a consequence of HF.[18] Here, we present evidence that cardiac-specific overexpression of the vasoactive agent ET-1 induces a progressive systemic cardiac conduction defect 'prior' to the development of HF. We have shown that as little as 4 weeks of ET-1 excess in the heart can trigger reduced Cx43, Cx40, and $Na_v1.5$ expression, reduced Na^+ channel conductance, and slow ventricular conduction, whereas the overall structure and contractile function of the heart remain essentially normal. If the ET-1 overexpression is left 'on', the scope and severity of the cardiac electrical dysfunction progress and overt HF develops by 8 weeks of ET-1 overexpression. Importantly, turning 'off' ET-1 overexpression at the onset of electrical remodelling was able to reverse the electrical dysfunction and prevent the development of HF.

4.1 Role of ET-1 in electrical remodelling

The cardiac voltage–gated sodium channel $Na_v1.5$ and the dominant gap junction channel in the working ventricular myocardium Cx43 are the key determinants of electrical impulse propagation.[19] Our study suggests that cardiac overexpression of ET-1 leads to impaired conduction (*Figure 3*) via Cx43 and $Na_v1.5$ remodelling (*Figure 4*). Although a recent *in vitro* study found that ET-1 led to 'increased' levels of Cx43 protein in neonatal rat ventricular myocytes, they, like us, also found 'reduced' intensity and expression of Cx43 associated with 'reduced' conduction velocity.[5] In agreement with our findings of reduced Cx43 phosphorylation at Ser368 correlating with impaired conduction, dephosphorylation of Cx43 at PKC consensus sites has been shown to impair gap junction conductance.[20] In astrocytes, ET-1 causes reduced Cx43 expression and gap-junctional intercellular communication associated with activated ET_B receptors.[21] Also, a study recently showed that a loss of Cx43 protein in rabbit LV myocytes similar to that shown in our model (40–70%) was associated with markedly reduced cell coupling.[22]

In addition, studies have shown that tumour necrosis factor α (TNFα), Na^+/H^+ exchange isoform–1, and activated c-Src may be linked with impaired Cx43 activity. TNFα has been shown to reduce Cx43 promoter activity in a rat myoblast cell line,[23] Na^+/H^+ exchange isoform–1 was shown to negatively regulate Cx43 expression through a JNK1/2-dependent pathway in neonatal rat ventricular myocytes,[24] and activated c-Src has been shown to reduce gap–junctional intercellular communication via tyrosine phosphorylation of Cx43.[25] In human ovarian carcinoma cells, ET-1-mediated gap junction uncoupling and reduced Cx43 expression are linked with increased tyrosine phosphorylation by c-Src via activated ET_AR[4]. As ET-1 stimulates TNFα in macrophages[26] and activates the Na^+/H^+ exchange isoform–1[7] and c-Src[27] in neonatal rat ventricular myocytes, it is possible that TNFα, Na^+/H^+ exchange isoform–1, or c-Src mediates the gap junction remodelling observed in our ET-1 overexpressing mice.

Cx43 is normally located at the intercalated disk (ID) in a multiprotein complex with N-cadherin and $Na_v1.5$ in ventricular myocytes, presumably working in collaboration for effective electrical coupling between cardiomyocytes. However, in human and animal models of HF, Cx43 mRNA and protein expression is reduced, and Cx43 dephosphorylation and lateralization are increased.[28] Unlike the reduced Cx43 levels seen in human HF, changes in Cx45 levels that accompany HF have been inconsistent.[29,30] The Purkinje fibres isolated from a canine model of ventricular tachy-pacing-induced HF exhibited delayed His–Purkinje conduction, decreased mRNA and protein expression of $Na_v1.5$ and Cx43, reduced Cx43 phosphorylation, and increased lateralization of Cx43.[31] Studies have shown that the association of Cx43 with zonula occludens-1 is increased in

Downloaded from cardiovascres.oxfordjournals.org at University of Toronto Library on March 1, 2011

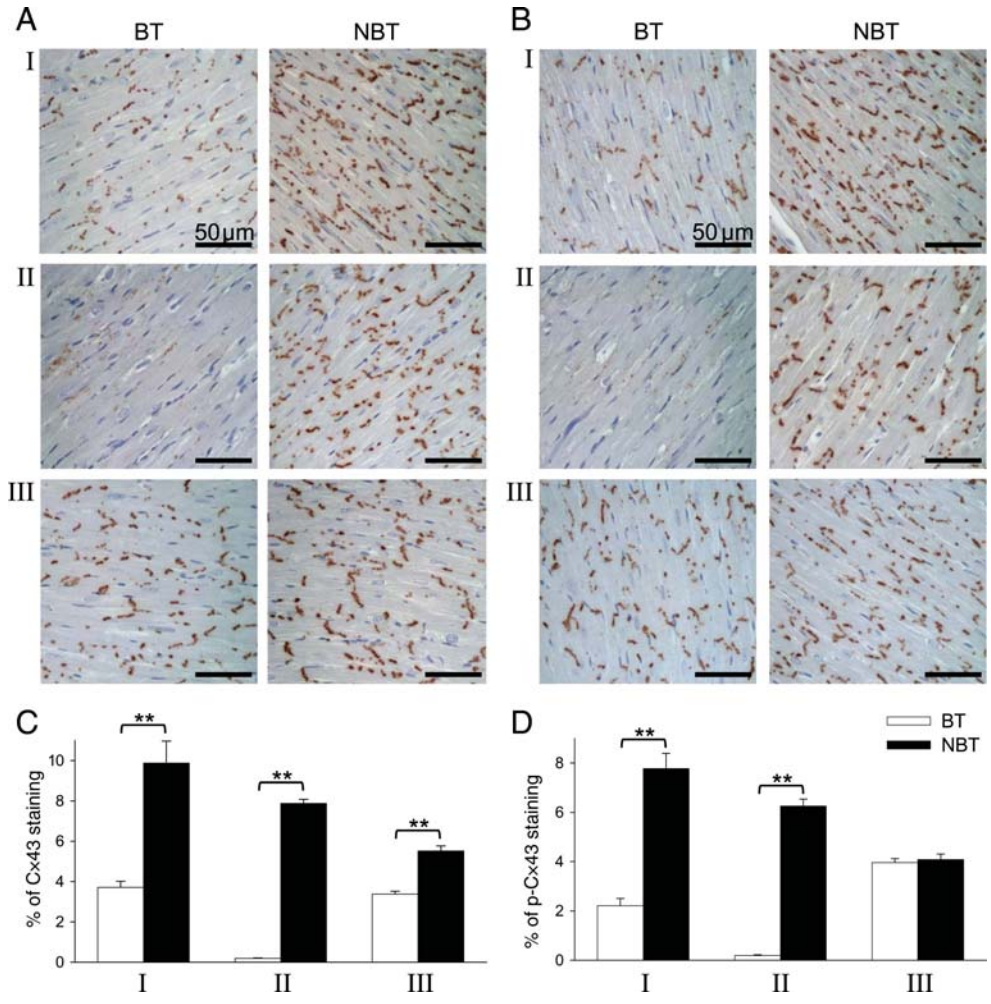

Figure 6 Prolonged ET-1 overexpression leads to progressive loss and lateralization of Cx43 and p-Cx43. Four weeks of ET-1 overexpression led to reduced Cx43 and p-Cx43 staining, whereas 8 weeks of overexpression caused reduced and lateralized Cx43 and p-Cx43 staining. Representative Cx43 (*A*) and p-Cx43 (*B*) staining of heart sections and % of Cx43 (*C*) and p-Cx43 staining (*D*) in BT and NBT mice from Groups I–III ($n = 2–5$ per genotype per group). $^{**}P < 0.01$.

human HF[32] and Cx43 lateralization and subsequent loss of Cxs from the ID is linked with increased association of zonula occludens-1 with activated c-Src.[33] However, in these studies, changes in Cx43 expression and localization were observed 'after' HF developed. Indeed, we believe that the current study represents the first report of how these changes in Cx43 localization can 'precede' HF, and how their reversal may prevent progression to HF.

Na^+ channel α- and β-subunits are localized to t-tubules and the ID. $Na_v1.5$ channels located at the ID are thought to play a key role in propagation of the action potential between cells, whereas Na^+ channels in t-tubules are involved in linking depolarization of the cell membrane with contraction. Scn5a (Na^+ type 5α−subunit) encodes the pore-forming α-subunit of the voltage-gated $Na_v1.5$ channel. Interestingly, only tyrosine phosphorylated β1-subunits are found with $Na_v1.5$ at the ID,[34] and normal functioning $Na_v1.5$ requires dystrophin at the ID as dystrophin-deficient mice have severely compromised levels of $Na_v1.5$ expression and increased QRS duration.[35] HF is also associated with reduced I_{Na}, a down-regulation of native $Na_v1.5$ mRNA, an up-regulation of two non-functional C-terminal splice variants, and reduced $Na_v1.5$ protein.[36] Mutations in Scn5a gene have been linked with impaired conduction and are associated with Lenègre disease, the Brugada syndrome, and long QT syndrome.[37] Indeed, $Scn5a^{+/-}$ mice develop impaired conduction, fibrosis, and diminished and disturbed distribution of Cx43.[38] A link between ET-1 overexpression and $Na_v1.5$ down-regulation can also be hypothesized based on our knowledge of ET-1 acting via NFκB-mediated transcription,[39] and a report of NFκB (p50) binding to and repressing activity of the Scn5a promoter.[40]

4.2 Electrical remodelling in the pathogenesis of HF

Electrical remodelling as a trigger for HF development as yet has not been firmly established. Studies have suggested that left bundle branch block may mediate LV dysfunction;[41] however, the molecular mechanism is unknown. Gap junction/ion channel remodelling leading to mechanical dysfunction in the heart represents a novel concept in the pathogenesis of HF. As electrical remodelling (*Figure 3*) and related molecular changes precede structural and functional remodelling (*Figure 4*), and as these events were reversible by suppressing ET-1

Downloaded from cardiovascres.oxfordjournals.org at University of Toronto Library on March 1, 2011

overexpression, our model supports the view that electrical remodelling at a molecular level can contribute to HF. The alternative interpretation is that ET-1 induces electrical remodelling first, and subsequently causes cardiac structural and functional deterioration through an entirely unrelated mechanism. The inability to selectively prevent the electrical remodelling-mediated molecular changes (reductions in Cx43 and $Na_v1.5$ expression) in mice overexpressing ET-1 presents a limitation for our study. Although ET-1-induced cytokine expression and fibrosis may also play a role in the pathogenesis of HF in our model,[11] the fact that the molecular and electrophysiological changes described here preceded any evidence of contractile dysfunction obtained using highly sensitive measures argues against later-stage inflammation and fibrosis being the only mechanisms involved. However, these mechanisms may have exacerbated the conduction delays in mice with HF.

Recently, mutations in Scn5a have been described leading to dilated cardiomyopathy with atrial/ventricular arrhythmia and impaired Ca^{2+} and Na^+ homeostasis with mechanical dysfunction.[42] Additionally, mice expressing a mutant form of Csx/Nkx2.5 under the β-MHC promoter develop conduction defects with down-regulation of Cx40/Cx43 and HF.[43] Although not emphasized in their report, the sequence of events again suggests that conduction defects develop 'prior' to any structural remodelling. However, down-regulation of Cx43 alone may be insufficient to cause HF as mice with cardiac-restricted deletion of Cx43 develop impaired ventricular conduction, spontaneous arrhythmias, and sudden cardiac death, but not overt HF.[44] Taken together, these data lead us to propose that electrical remodelling leading to HF require both reduced expression and/or phosphorylation of Cx43 as well as impaired $Na_v1.5$ function at the ID.

In conclusion, our study suggests that in the heart, ET-1 leads to impaired conduction via gap junction/ion channel remodelling. The sequence and reversibility of this cardiomyopathy phenotype suggests that a primary abnormality in electrophysiology may trigger subsequent ventricular dysfunction and may represent a therapeutic target in HF. This conceptual paradigm deserves closer examination in human HF, particularly in conditions where early 'electrical' interventions may be tested for their ability to prevent the progression to, or possibly even reverse, the manifestations of ventricular dysfunction.

Supplementary material

Supplementary material is available at *Cardiovascular Research* online.

Conflict of interest: none declared.

Funding

This work was supported by operating grants from the Canadian Institutes of Health Research (MOP74752 to M.H. and D.J.S and MOP153103 to P.H.B.) and the Heart and Stroke Foundation of Ontario (T5536 to M.H. and D.J.S. and T6485 to P.H.B.); an Ontario Graduate Scholarship in Science and Technology to E.E.M.; and a Career Investigator of the Heart and Stroke Foundation of Ontario (5503 to M.H. and CI6841 to P.H.B.)

References

1. Schiffrin EL. Beyond blood pressure: the endothelium and atherosclerosis progression. *Am J Hypertens* 2002;**15**:115S–122S.
2. Yang LL, Arab S, Liu P, Stewart DJ, Husain M. The role of endothelin-1 in myocarditis and inflammatory cardiomyopathy: old lessons and new insights. *Can J Physiol Pharmacol* 2005;**83**:47–62.
3. Polontchouk L, Ebelt B, Jackels M, Dhein S. Chronic effects of endothelin 1 and angiotensin II on gap junctions and intercellular communication in cardiac cells. *FASEB J* 2002;**16**:87–89.
4. Spinella F, Rosano L, Di Castro V, Nicotra MR, Natali PG, Bagnato A. Endothelin-1 decreases gap junctional intercellular communication by inducing phosphorylation of connexin 43 in human ovarian carcinoma cells. *J Biol Chem* 2003;**278**:41294–41301.
5. Reisner Y, Meiry G, Zeevi-Levin N, Barac DY, Reiter I, Abassi Z et al. Impulse conduction and gap junctional remodelling by endothelin-1 in cultured neonatal rat ventricular myocytes. *J Cell Mol Med* 2009;**13**:562–573.
6. Boixel C, Dinanian S, Lang-Lazdunski L, Mercadier JJ, Hatem SN. Characterization of effects of endothelin-1 on the L-type Ca^{2+} current in human atrial myocytes. *Am J Physiol Heart Circ Physiol* 2001;**281**:H764–H773.
7. Dulce RA, Hurtado C, Ennis IL, Garciarena CD, Alvarez MC, Caldiz C et al. Endothelin-1 induced hypertrophic effect in neonatal rat cardiomyocytes: involvement of Na^+/H^+ and Na^+/Ca^{2+} exchangers. *J Mol Cell Cardiol* 2006;**41**:807–815.
8. Izumi T, Kihara Y, Sarai N, Yoneda T, Iwanaga Y, Inagaki K et al. Reinduction of T-type calcium channels by endothelin-1 in failing hearts *in vivo* and in adult rat ventricular myocytes *in vitro*. *Circulation* 2003;**108**:2530–2535.
9. Kiesecker C, Zitron E, Scherer D, Lueck S, Bloehs R, Scholz EP et al. Regulation of cardiac inwardly rectifying potassium current IK1 and Kir2.x channels by endothelin-1. *J Mol Med* 2006;**84**:46–56.
10. Matsumoto Y, Aihara H, Yamauchi-Kohno R, Reien Y, Ogura T, Yabana H et al. Long-term endothelin a receptor blockade inhibits electrical remodeling in cardiomyopathic hamsters. *Circulation* 2002;**106**:613–619.
11. Yang LL, Gros R, Kabir MG, Sadi A, Gotlieb AI, Husain M et al. Conditional cardiac overexpression of endothelin-1 induces inflammation and dilated cardiomyopathy in mice. *Circulation* 2004;**109**:255–261.
12. Zhu W, Saba S. Cardiac electrophysiologic abnormalities in the CREBA133 transgenic mouse model of idiopathic dilated cardiomyopathy. *J Cardiovasc Electrophysiol* 2003;**14**:982–989.
13. Ju H, Gros R, You X, Tsang S, Husain M, Rabinovitch M. Conditional and targeted overexpression of vascular chymase causes hypertension in transgenic mice. *Proc Natl Acad Sci USA* 2001;**98**:7469–7474.
14. Zhou YQ, Foster FS, Nieman BJ, Davidson L, Chen XJ, Henkelman RM. Comprehensive transthoracic cardiac imaging in mice using ultrasound biomicroscopy with anatomical confirmation by magnetic resonance imaging. *Physiol Genomics* 2004;**18**:232–244.
15. Kasi VS, Xiao HD, Shang LL, Iravanian S, Langberg J, Witham EA et al. Cardiac-restricted angiotensin-converting enzyme overexpression causes conduction defects and connexin dysregulation. *Am J Physiol Heart Circ Physiol* 2007;**293**:H182–192.
16. Zaheer A, Sahu SK, Wu Y, Zaheer A, Haas J, Lee K et al. Diminished cytokine and chemokine expression in the central nervous system of GMF-deficient mice with experimental autoimmune encephalomyelitis. *Brain Res* 2007;**1144**:239–247.
17. Gros R, Afroze T, You XM, Kabir G, Van Wert R, Kalair W et al. Plasma membrane calcium ATPase overexpression in arterial smooth muscle increases vasomotor responsiveness and blood pressure. *Circ Res* 2003;**93**:614–621.
18. Nattel S, Maguy A, Le Bouter S, Yeh YH. Arrhythmogenic ion-channel remodeling in the heart: heart failure, myocardial infarction, and atrial fibrillation. *Physiol Rev* 2007;**87**:425–456.
19. Kucera JP, Rohr S, Rudy Y. Localization of sodium channels in intercalated disks modulates cardiac conduction. *Circ Res* 2002;**91**:1176–1182.
20. Solan JL, Lampe PD. Connexin43 phosphorylation: structural changes and biological effects. *Biochem J* 2009;**419**:261–272.
21. Rozyczka J, Figiel M, Engele J. Chronic endothelin exposure inhibits connexin43 expression in cultured cortical astroglia. *J Neurosci Res* 2005;**79**:303–309.
22. Ai X, Zhao W, Pogwizd SM. Connexin43 knockdown or overexpression modulates cell coupling in control and failing rabbit left ventricular myocytes. *Cardiovasc Res* 2010;**85**:751–762.
23. Fernandez-Cobo M, Gingalewski C, Drujan D, De Maio A. Downregulation of connexin 43 gene expression in rat heart during inflammation. The role of tumour necrosis factor. *Cytokine* 1999;**11**:216–224.
24. Stanbouly S, Kirshenbaum LA, Jones DL, Karmazyn M. Sodium hydrogen exchange 1 (NHE-1) regulates connexin 43 expression in cardiomyocytes via reverse mode sodium calcium exchange and c-Jun NH_2-terminal kinase-dependent pathways. *J Pharmacol Exp Ther* 2008;**327**:105–113.
25. Toyofuku T, Yabuki M, Otsu K, Kuzuya T, Tada M, Hori M. Functional role of c-Src in gap junctions of the cardiomyopathic heart. *Circ Res* 1999;**85**:672–681.
26. Ruetten H, Thiemermann C. Endothelin-1 stimulates the biosynthesis of tumour necrosis factor in macrophages: ET-receptors, signal transduction and inhibition by dexamethasone. *J Physiol Pharmacol* 1997;**48**:675–688.
27. Kovacic B, Ilic D, Damsky CH, Gardner DG. c-Src activation plays a role in endothelin-dependent hypertrophy of the cardiac myocyte. *J Biol Chem* 1998;**273**:35185–35193.

Downloaded from cardiovascres.oxfordjournals.org at University of Toronto Library on March 1, 2011

28. Severs NJ, Bruce AF, Dupont E, Rothery S. Remodelling of gap junctions and connexin expression in diseased myocardium. *Cardiovasc Res* 2008;**80**:9–19.
29. Yamada KA, Rogers JG, Sundset R, Steinberg TH, Saffitz JE. Up-regulation of connexin45 in heart failure. *J Cardiovasc Electrophysiol* 2003;**14**:1205–1212.
30. Dupont E, Matsushita T, Kaba RA, Vozzi C, Coppen SR, Khan N et al. Altered connexin expression in human congestive heart failure. *J Mol Cell Cardiol* 2001;**33**: 359–371.
31. Maguy A, Le Bouter S, Comtois P, Chartier D, Villeneuve L, Wakili R et al. Ion channel subunit expression changes in cardiac Purkinje fibers: a potential role in conduction abnormalities associated with congestive heart failure. *Circ Res* 2009;**104**:1113–1122.
32. Bruce AF, Rothery S, Dupont E, Severs NJ. Gap junction remodelling in human heart failure is associated with increased interaction of connexin43 with ZO-1. *Cardiovasc Res* 2008;**77**:757–765.
33. Kieken F, Mutsaers N, Dolmatova E, Virgil K, Wit AL, Kellezi A et al. Structural and molecular mechanisms of gap junction remodeling in epicardial border zone myocytes following myocardial infarction. *Circ Res* 2009;**104**:1103–1112.
34. Malhotra JD, Thyagarajan V, Chen C, Isom LL. Tyrosine-phosphorylated and nonphosphorylated sodium channel beta1 subunits are differentially localized in cardiac myocytes. *J Biol Chem* 2004;**279**:40748–40754.
35. Gavillet B, Rougier JS, Domenighetti AA, Behar R, Boixel C, Ruchat P et al. Cardiac sodium channel Nav1.5 is regulated by a multiprotein complex composed of syntrophins and dystrophin. *Circ Res* 2006;**99**:407–414.
36. Shang LL, Pfahnl AE, Sanyal S, Jiao Z, Allen J, Banach K et al. Human heart failure is associated with abnormal C-terminal splicing variants in the cardiac sodium channel. *Circ Res* 2007;**101**:1146–1154.
37. Royer A, van Veen TA, Le Bouter S, Marionneau C, Griol-Charhbili V, Leoni AL et al. Mouse model of SCN5A-linked hereditary Lenegre's disease: age-related conduction slowing and myocardial fibrosis. *Circulation* 2005;**111**:1738–1746.
38. van Veen TA, Stein M, Royer A, Le Quang K, Charpentier F, Colledge WH et al. Impaired impulse propagation in Scn5a-knockout mice: combined contribution of excitability, connexin expression, and tissue architecture in relation to aging. *Circulation* 2005;**112**:1927–1935.
39. Hirotani S, Otsu K, Nishida K, Higuchi Y, Morita T, Nakayama H et al. Involvement of nuclear factor-kappaB and apoptosis signal-regulating kinase 1 in G-protein-coupled receptor agonist-induced cardiomyocyte hypertrophy. *Circulation* 2002;**105**:509–515.
40. Shang LL, Sanyal S, Pfahnl AE, Jiao Z, Allen J, Liu H et al. NF-kappaB-dependent transcriptional regulation of the cardiac scn5a sodium channel by angiotensin II. *Am J Physiol Cell Physiol* 2008;**294**:C372–C379.
41. Liu L, Tockman B, Girouard S, Pastore J, Walcott G, KenKnight B et al. Left ventricular resynchronization therapy in a canine model of left bundle branch block. *Am J Physiol Heart Circ Physiol* 2002;**282**:H2238–H2244.
42. Nguyen TP, Wang DW, Rhodes TH, George AL Jr. Divergent biophysical defects caused by mutant sodium channels in dilated cardiomyopathy with arrhythmia. *Circ Res* 2008;**102**:364–371.
43. Kasahara H, Wakimoto H, Liu M, Maguire CT, Converso KL, Shioi T et al. Progressive atrioventricular conduction defects and heart failure in mice expressing a mutant Csx/Nkx2.5 homeoprotein. *J Clin Invest* 2001;**108**:189–201.
44. Gutstein DE, Morley GE, Tamaddon H, Vaidya D, Schneider MD, Chen J et al. Conduction slowing and sudden arrhythmic death in mice with cardiac-restricted inactivation of connexin43. *Circ Res* 2001;**88**:333–339.

Downloaded from cardiovascres.oxfordjournals.org at University of Toronto Library on March 1, 2011